Effects of structural parameters on water film properties of transpiring wall reactor

Donghai Xu*, Peng Feng, Yang Wang, Wanpeng Yang, Yu Wang, Shaoyan Sun

Key Laboratory of Thermo-Fluid Science & Engineering, Ministry of Education, School of Energy and Power Engineering, Xi'an Jiaotong University, Xi'an, Shaanxi Province, 710049, China

Abstract: Reactor corrosion and salt deposition problems severely restrict the industrialization of supercritical water oxidation. Transpiring wall reactor can effectively weaken these two problems through a protective water film formed on its internal surface. In this work, the effects of key structural parameters on water film properties of transpiring wall reactor were explored by numerical simulation, and established models were validated by comparing simulation and experimental values. The results show that transpiration water layer, transpiring wall porosity and inner diameter hardly affected organic matter degradation. Increasing transpiration water layer and transpiring wall porosity reduced reactor center temperatures in the middle and lower zones of the reactor. Increasing transpiration water layer, transpiring wall porosity and inner diameter decreased water film temperatures but increased water film coverage rates. Increasing reactor length affected slightly on the volume of the upper supercritical oxidation zone but enlarged the subcritical zone.

Keywords: supercritical water oxidation, transpiring wall reactor, water film, structural parameter, numerical simulation

一 Introduction

Supercritical water oxidation (SCWO) can remove organic wastes rapidly and efficiently through unique properties of supercritical water (T> 647 K, P> 22.1 MPa). However, inorganic salts easily deposit in the reactor in supercritical water due to their very low solubilities [1-3], thereby causing pressure fluctuation, reactor plugging, frequent shutdowns and so on [1]. Meanwhile, various corrosion substances derived from feedstock and/or reaction products probably result in severe reactor corrosion problems in SCWO [4, 5]. Transpiring wall reactor (TWR) is a promising reactor type to effectively overcome the two problems above via a protective water film formed on the internal surface of the reactor [6-7].

Apparently, structural parameters are vital factors of affecting water film properties of TWR [9]. Some kinds of TWRs with different structural designs have been developed in the past decade. However, the investigations on effects of various structural parameters on water film properties are relatively scare now. Chen et al. [10] studied the fluid dynamics of transpiring flow to provide the foundation for the design and optimization of a TWR. Zhang et al. [9] reported that increasing reactor diameter and length promoted feed degradation, and a lower length/diameter (H/D) ratio at a constant volume was more beneficial for water film formation and feed degradation. Bermejo et al. [11, 12] carried out TWR research by developing

* Corresponding author: Tel: +86-29-82665749; Fax: +86-29-8266-8703.

E-mail addresses: xudonghai@mail.xjtu.edu.cn (Donghai Xu).

transpiring wall structures and materials, and confirmed that the influences of the upper transpiring wall made of a porous material on reactor performance were limited. Prikopsky et al. [13] claimed that different porosities (17% and 21%) did not significantly affect salt accumulation in the reactor. However, our previous work found that fluid flow characteristics in a TWR could be affected by its porosity [4]. Overall, now it is still lack of a comprehensive and in-depth cognition concerning the effects of various structural parameters on organic matter degradation and water film properties in TWRs.

This work aims to systematically explore the effects of key structural parameters (i.e., transpiring wall porosity, transpiration water layer, transpiring wall inner diameter and reactor length) on water film properties of a TWR. To the best of our knowledge, this is documented for the first time. This information is valuable for guiding water film formation with good corrosion and salt deposition resistance.

二 Model and verification

二.1 Physical model and boundary conditions

Fig. 1 illustrates a two-dimensional axisymmetric physical model established for the TWR in this work. Simulation area was limited inside the pressure-bearing wall of the reactor. Methanol solution (i.e., organic feedstock) and oxygen were stably injected into the reactor via its top inlet after preheated and mixed evenly. Transpiration water was injected into the reactor's annular space through the inlets of transpiration water at constant speed and temperature. An electric heating device around the reactor's external surface was used to maintain a desired temperature during the whole reaction process, and so the pressure-bearing internal wall could be regarded as adiabatic boundary. Except for heat conduction effect of the porous transpiring wall, other solid walls were set as adiabatic boundaries as well.

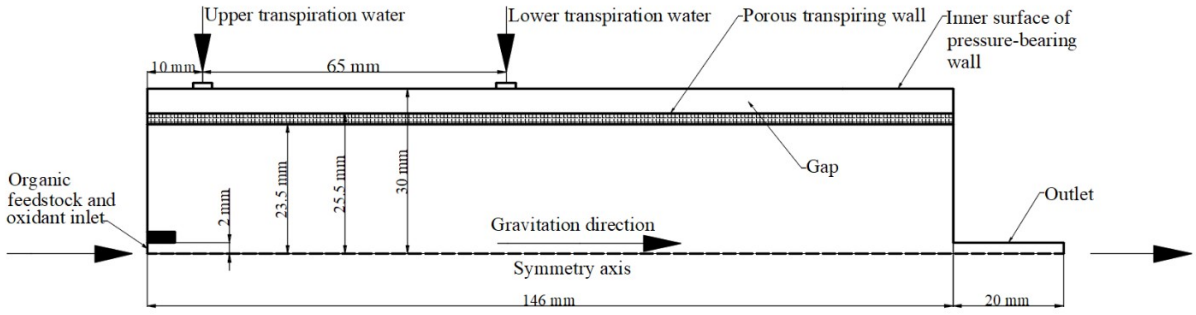

Fig. 1 Simplified physical model for TWR.

Simulation area was discretized through structural quadrilateral grids, of which total number was 1.5×10^5. Boundary layer was densified on the internal surface of the porous transpiring wall to improve calculation accuracy, and grid independence verification was conducted to eliminate computational errors. Mass entrance boundary was adopted for organic feed, oxidant or transpiration water, while pressure boundary was used for the reactor bottom outlet. Notably, the reactor was maintained at 23 MPa throughout reaction processes.

二.2 Simulation method

The SCWO processes of organic matters in a TWR involve multi-component mixture flow, heat and mass transfer, and chemical reactions [14]. Fluid flow in most regions was in the turbulent state, and physical properties varied sharply in the trans-critical zone. The RNG k-ε model based on the Renormalization

Group (RNG) method can be well suitable for the flow field with circulation region, strong swirl, and high velocity gradient due to its high accuracy [15]. Hence, it was selected as the turbulence model for turbulence calculation near the transpiring wall of the TWR in this work.

The oxidation reactions of methanol and oxygen in SCWO in the TWR leads to the formation of CO_2 and water. The corresponding reaction rate was calculated by the Arrhenius equation,

$$2CH_3OH+3O_2 \rightarrow 2CO_2+4H_2O \quad r=-c_{CH_3OH}^{n} c_{O_2}^{m} A \exp\left(\frac{-E_a}{RT}\right) \tag{1}$$

where pre-exponential factor (A), activation energy (E_a), methanol reaction order (n), and oxygen reaction order (m) are $1\times10^{26.2}$, 408.8 kJ·mol^{-1}, 1 and 0, respectively [16], R (J·K^{-1}·mol^{-1}) is gas constant, and T (K) is reaction temperature. Finite rate/eddy dissipation model is suitable for complex oxidation reactions in the TWR, and thus selected as the reaction kinetics model in this research.

The flow velocity of transpiration water was relatively low, and its temperature was in a subcritical state. Moreover, there were also not chemical reactions in the transpiring wall. Hence, the flow in the porous transpiring wall mainly belonged to a viscous flow, which conforms the Darcy's law [17],

$$\Delta p=\frac{Q\delta'}{A_S}\left(\frac{\mu}{\alpha}+\frac{Q\rho}{\beta' A_S}\right) \tag{2}$$

where Δp (MPa) is the pressure drop through the porous transpiring wall, Q (m^3·s^{-1}) is the volume flow rate of fluid, δ' (m) is the thickness of the transpiring wall, A_S (m^2) is circulation area, μ (Pa·s^{-1}) is dynamic viscosity, α is viscosity coefficient, ρ (kg·m^{-3}) is density, and β' is inertial coefficient.

二.3 Model verification

Temperature field reflects reaction processes in the reactor, and is one of key factors affecting water film properties. Six temperature measuring points were installed in supercritical (L = 40 mm) and subcritical zones (L = 121 mm) from the reactor top along the axis direction. The measured temperatures can be compared with simulation values to verify the accuracy of mathematical models. As displayed in **Table 1**, simulation results were slightly higher than experimental values under the same conditions. However, relative errors were lower than 6.5%, corresponding to absolute errors of < 40 K. This is mainly attributed to some simplified assumptions, such as adiabatic boundary of external TWR surface, complete reaction of organic matters and oxygen, and linear input of physical parameters near the water critical point. Overall, the good agreement between experiment and simulation temperatures here shows that the numerical models established in this research are reasonable and reliable within acceptable errors.

Table 1 Comparison of experiment and simulation temperatures under the conditions of $p=$ 23 MPa, $Q_m=$ ¿0.95 L·h-

1

$T_{feed}=$ 703 K, $\alpha_m=20\%, \delta=0.35$, $T_t=543$ K, $\chi=1.25$, $\gamma=2, d_t=47\,mm, L=146\,mm \wedge \beta=0.35$

.

Radial distance (mm)	Reactor length L = 40 mm			Reactor length L = 121 mm		
	Simulation value (K)	Experiment value (K)	Relative error (%)	Simulation value (K)	Experiment value (K)	Relative error (%)

12	715.4	693.0	3.2	606.5	589.4	2.8
17	704.0	674.8	4.2	601.4	574.9	4.4
22	683.5	662.7	3.0	596.5	560.2	6.1

二.4 Definition and evaluation of physical parameters

For a pure component, density can be calculated via the P-R equation [18], while specific heat capacity, thermal conductivity and viscosity coefficient are obtained from the NIST database. Reactants and products are mixtures in the TWR, and their physical parameters are able to be evaluated by the weighted average of pure components. The diffusion coefficient of mixture can be determined by that of each component and its proportion. Apparently, water is the main component in SCWO in the TWR, and its proportion is far higher than the sum of other components. Thus, the diffusion coefficient of supercritical fluid can be approximately expressed by that of pure water under the same conditions (see Eq. (3)) [19],

$$D=\frac{A(T)+B(T)\rho_{\mathrm{mol}}\ln\rho_{\mathrm{mol}}+C(T)\rho_{\mathrm{mol}}+E(T)\rho_{\mathrm{mol}}^{1.3613}}{10^{4}} \tag{3}$$

$$\rho_{\mathrm{mol}}=\frac{\rho}{10^{3}\times M} \tag{4}$$

$$A(T)=\frac{7.59322\times T^{0.45456}}{10^{7}} \tag{5}$$

$$B(T)=0.00142704+\frac{0.223153}{T}-\frac{0.24277\times T}{10^{5}} \tag{6}$$

$$C(T)=0.0085568+\frac{0.859735}{T}-\frac{0.12813\times T}{10^{4}} \tag{7}$$

$$E(T)=-0.018153+\frac{0.029224\times T}{10^{3}}-\frac{0.0083486\times T^{2}}{10^{6}} \tag{8}$$

where D ($m^2 \cdot s^{-1}$) is diffusion coefficient, ρ_{mol} ($mol \cdot cm^{-3}$) is molar density, *A(T)*, *B(T)*, *C(T)* and *E(T)* are temperature coefficients, ρ ($kg \cdot m^{-3}$) is density, T (K) is temperature, and M ($g \cdot mol^{-1}$) is molar mass.

Both pressure-bearing wall and transpiring wall of TWR are made of 316 stainless steel, and their thermal conductivities affect heat transfer in the reactor. Specific heat capacity (c_p) at a constant pressure and thermal conductivity (λ) can be calculated by Eqs. (9) and (10), respectively [20].

$$c_p=\frac{13.6\times T}{100}-\frac{2.82\times 10^{6}}{T^{2}}+472 \tag{9}$$

$$\lambda=0.0175\times T-\frac{2\times T^{2}}{10^{6}}+9.2 \tag{10}$$

The thermal conductivity (λ') of the porous transpiring wall is related with fluid and porosity,

$$\lambda'=\beta\lambda_f+(1-\beta\lambda_s) \tag{11}$$

where β is the porosity of the transpiring wall, λ_f ($W \cdot m^{-1} \cdot K^{-1}$) is the thermal conductivity of fluid, and λ_s ($W \cdot m^{-1} \cdot K^{-1}$) is the thermal conductivity of solid.

Water film coverage rate (R_f) represents the content of transpiration water in the water film, and can be evaluated by Eq. (12),

$$R_f = \frac{Q_t}{Q_{tot}} \tag{12}$$

where Q_t (L·h^{-1}) is the flow rate of transpiration water at one location on the inner surface of the transpiring wall, and Q_{tot} (L·h^{-1}) is the total flow rate of fluid (including transpiration water, organic feedstock and oxidant) at the location.

Transpiring wall porosity (β) refers to the ratio of pore volume to transpiring wall's total volume,

$$\beta = \frac{-V_e}{V_t} \tag{13}$$

where V_e (m^3) is the pore volume of transpiring wall, and V_t (m^3) is the total volume of transpiring wall.

Furthermore, water film temperature (T_f) refers to the average temperature of fluid in water film. Reactor center temperature (T_c) represents the temperature in the reactor geometric center, and changes at different reactor length (L) locations. It can be used to define supercritical length ($L_{¿}$) and subcritical length ($L_{¿}$) zones of the reactor. Transpiration water layer (γ) means that transpiration water is pumped into the reactor via inlets located on several layers.

三 Results and discussions

三.1 Influence of transpiring wall porosity

Transpiring wall porosity (β) is one of key structural parameters affecting the flow resistance of transpiration water [21, 22]. Internal resistance coefficient (η) and permeability (ζ) are two significant factors to characterize the flow resistance above [23], and can be obtained via the Darcy's law [17] and basic formulas of fluid flow. Internal resistance coefficient and permeabilities at various porosities conditions can be seen in **Table 2**. These values can be input into the panels of porous media models during simulation processes.

Table 2 Internal resistance coefficients and permeabilities at various porosities conditions.

Item	β = 0.2	β = 0.3	β = 0.4	β = 0.5
η (m^{-1})	1.46 E+07	3.78 E+06	1.37 E+06	5.83 E+05
ζ (m^2)	2.40 E–13	7.05 E–13	1.71 E–12	3.84 E–12

Fig. 2 illustrates temperature field distributions at various porosities conditions (i.e., 0.2 – 0.5). Apparently, turbulent mixing and high-temperature reaction zones approached the reactor top inlet, and subcritical salt-dissolving zone expanded as transpiring wall porosity increased. This can be explained by the fact that increasing transpiring wall porosity decreased internal resistance coefficient but increased permeability [23] (see **Table 2**), and thereby transpiration water can diffuse more easily through the transpiring wall. As a result, a larger subcritical salt-dissolving zone was formed in the middle and lower zones of the reactor. However, Bermejo and Prikopsky et al. [12, 13] reported that the influences on reactor performance was limited when the upper transpiring wall was made of a porous material. This phenomenon may be mainly attributed to different models and operating conditions.

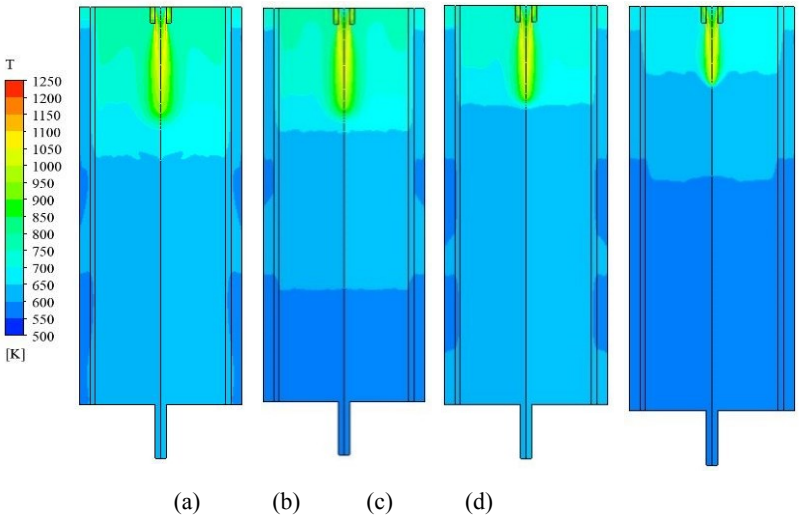

Fig. 2 Temperature field distributions at various transpiring wall porosities and $p = 23$ MPa, $Q_m = 0.95\ \mathrm{L \cdot h^{-1}}$, $T_{feed} = 753$ K, $\alpha_m = 20\%$, $\delta = 0.35$, $T_t = 543$ K, $\chi = 1.25$, $\gamma = 2$, $d_t = 47\ mm$, $\wedge L = 146\ mm$. (a) $\beta = 0.2$, (b) $\beta = 0.3$, (c) $\beta = 0.4$, (d) $\beta = 0.5$.

Fig. 3 displays reactor center temperatures and methanol concentrations at different transpiring wall porosities conditions. Obviously, the methanol concentration reduced to approximately zero near the reactor top inlet (L = 0.03 m) rapidly after organic feed entered into the reactor, so transpiring wall porosity hardly affected methanol degradation in SCWO. Reactor center temperatures increased to the maximum value at approximately L = 0.03 m, showing that rapid and thorough SCWO oxidation reactions occur and a large amount of heat is released around the reactor inlet [24]. Overall, reactor center temperature decreased with transpiring wall porosity increasing, and dramatically reduced especially in the range of L = 0.03 – 0.058 m owing to the cooling effect of low-temperature transpiration water. Notably, transpiring wall porosities slightly affected reactor center temperatures at β = 0.4 and 0.5 for the reactor length of L > 0.058 m. This can be attributed to the stable subcritical salt-dissolving zone in the lower zone of the reactor. The highest temperature position in the reactor moved upwards at β = 0.5, which is conducive to avoiding contacting corrosive species and possible organic salts in actual application.

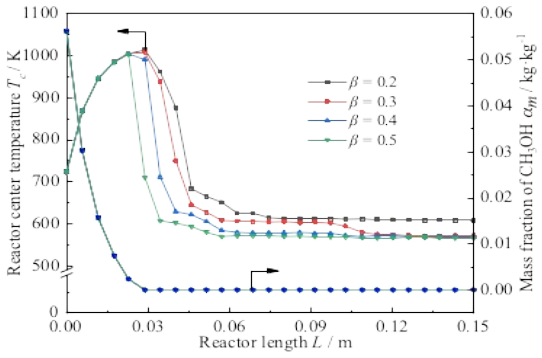

Fig. 3 Reactor center temperatures and methanol concentrations at various transpiring wall porosities and $p = 23$ MPa,

Q_m

¿0.95 L·h^{-1}, T_{feed} = 753 K, α_m=20%, δ=0.35, T_t=543 K, χ=1.25, γ=2, d_t=47 mm, $\wedge L$=146 mm

.

Fig. 4 elucidates water film temperatures and coverage rates under various transpiring wall porosities conditions. On the whole, the decreasing tendency was demonstrated for water film temperature along reactor length owing to the cooling effect of low-temperature transpiration water. It can be also observed from **Fig. 4** that water film temperature reduced remarkably with an increase in transpiring wall porosity, which increases the subcritical water film length. This is beneficial to forming a high-quality and continuous water film [14]. Notably, water film temperatures slightly decreased with transpiring wall porosity increasing at β > 0.3 for the reactor length of L > 0.06 m. Apparently, water film coverage rates increased with transpiring wall porosity increasing in the upper and middle zones (especially in the range of L = 0.015 – 0.045 m). However, high porosity inevitably reduced reactor temperature, thereby reducing the degradation ability of organic wastes. It is noteworthy that water film coverage rate was relatively stable in the middle and lower zones (L > 0.06 m). The reason may be that the stable subcritical salt-dissolving zone is formed in the lower zone of the reactor.

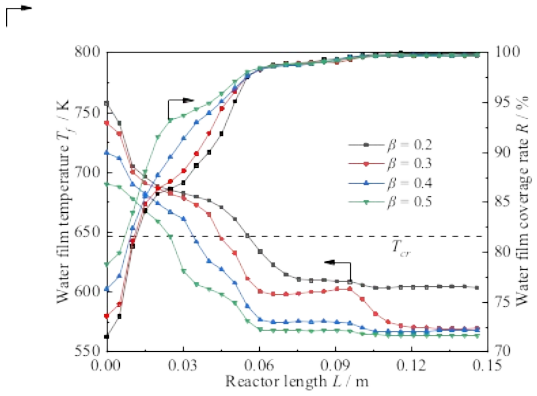

Fig. 4 Water film temperatures and coverage rates at various transpiring wall porosities and

p= 23 MPa, Q_m=0.95 L·h^{-1},

T_{feed} = 753 K, α_m=20%, δ=0.35, T_t=543 K, χ=1.25 γ=2, d_t=47 mm, $\wedge L$=146 mm.

三.2 Influence of transpiration water layer

Transpiration water layer (γ) significantly affects the uniformity and continuity of water film in the reactor, and thus influences reactor performance against reactor corrosion and salt deposition. **Fig. 5** displays the simplified reactor physical models under various transpiration water layers conditions. Transpiration water can be introduced into the TWR by various inlets located on different transpiration water layers on the pressure-bearing wall.

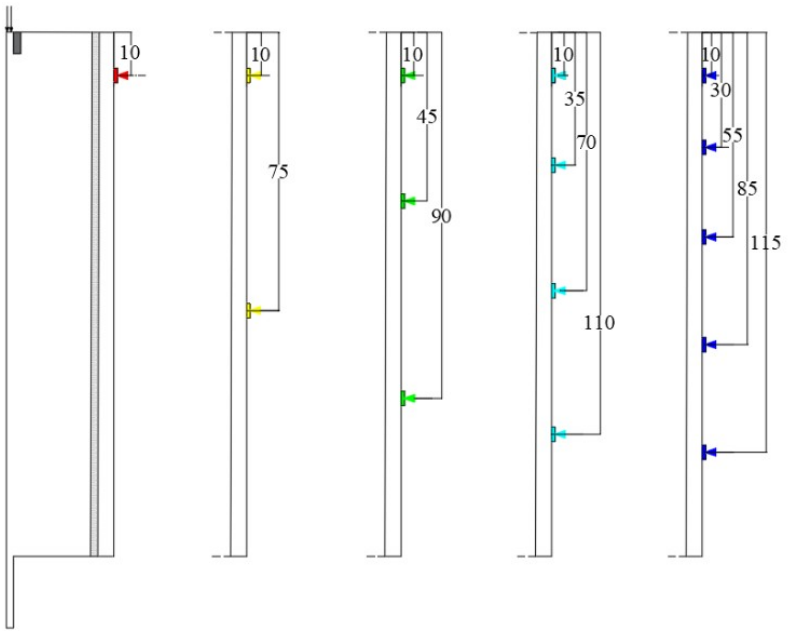

(a) (b) (c) (d) (e)

Fig. 5 Simplified reactor physical models at various transpiration water layers. (a)γ = 1, (b)γ = 2, (c)γ = 3, (d)γ = 4, (e)γ = 5.

Fig. 6 illustrates reactor center temperatures and methanol concentrations under different transpiration water layers conditions. Obviously, transpiration water layers almost had no impact on methanol concentrations. Reactor center temperatures were also hardly affected by transpiration water layers from the reactor top inlet to the L = 0.03 m location. The reason can be explained by the fact that the temperature and flow field distributions in high-temperature reaction zone near the reactor top inlet are mainly controlled by organic feed reactions (operating parameters of organic feedstock in essence) [25]. However, reactor center temperature reduced as transpiration water layer increased in the middle and lower zones (L > 0.03 m). This is likely attributed to the fact that increasing transpiration water layer can improve the distribution uniformity and continuity of water film. Notably, the whole reactor zone was in supercritical state at γ = 1, which is unconducive to forming an excellent water film to dissolve inorganic salts and corrosive substances [21]. It can be also found that transpiration water layer hardly affected reactor center temperature at γ > 3. Inevitably, much high porosity and many transpiration water pipelines significantly reduce system stability and safety. Hence, a proper selection for transpiration water layer requires to comprehensively take into account many factors above.

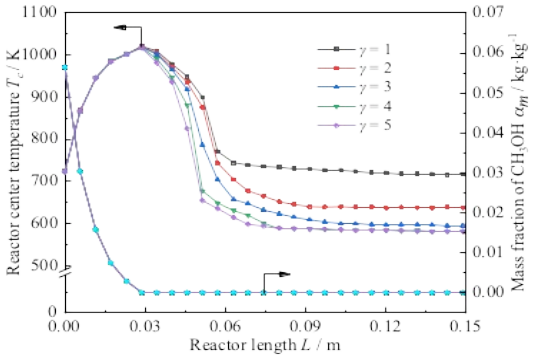

Fig. 6 Reactor center temperatures and methanol concentrations at various transpiration water layers and

$$p = 23\ \text{MPa}, Q_m$$

¿0.95 L·h^{-1}, T_{feed} = 753 K, α_m=20%, δ=0.35, T_t=543 K, χ=1.25 β=0.35, d_t=47 mm, $\wedge L$=146 mm

.

Fig 7 describes water film temperatures and coverage rates under different transpiration water layers conditions. As shown in **Fig. 7a**, water film temperature reduced but subcritical water film length increased dramatically with transpiration water layers increasing (especially at γ = 3, 4 or 5). This can be explained by the fact that several layers of transpiration water can diffuse through the porous transpiring wall more easily to form a continuous water film on the whole transpiring wall, so providing a low-temperature protection for the reactor. Notably, the whole water film was in supercritical state at γ = 1, and water film temperature increased along reactor length in the range of L = 0.08 – 0.14 m. The reason is that all of transpiration water enters the reactor through the upper inlet (see **Fig. 5a**), and results in the nonuniform distribution of transpiration water. However, the influences of transpiration water layer were limited at γ = 3, 4 or 5. Herein, two transpiration water layers (γ = 2), was recommended for the TWR in this work.

As displayed in **Fig. 7b**, water film coverage rates slightly varied with transpiration water layers increasing from the reactor top inlet to L = 0.015 m. It is probably explained by that water film distribution near the reactor top inlet is mainly determined by organic feed reactions [25]. However, transpiration water layers significantly affected water film coverage rages below L = 0.015 m. Water film coverage rate was only approximately 85% at γ = 1, which is unconducive to dissolving inorganic salts and corrosive substances [21].

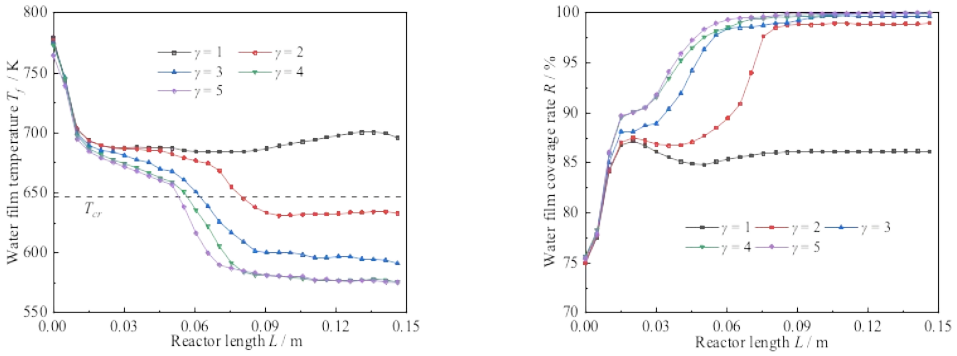

a) b)

Fig. 7 Water film temperatures and coverage rates at different transpiration water layers and

$$p = 23\ \text{MPa}, Q_m = 0.95\ \text{L}\cdot h^{-1},$$

$$T_{feed} = 753\ \text{K},\ \alpha_m = 20\%, \delta = 0.35,\ T_t = 543\ \text{K}, \chi = 1.25,\ \beta = 0.35, d_t = 47\ mm, \wedge L = 146\ mm.$$

三.3 Influence of transpiring wall inner diameter

Transpiring wall inner diameter (d_t) determines the reactor volume and the internal surface area of transpiring wall under a certain reactor length condition, thereby affecting the organic feed degradation, and heat and mass transfer between bulk fluid and transpiration water. Herein, it is assumed that transpiration water diffusion in the annulus was the same at various inner diameters, and the dissipation in the annulus was ignored. Thus, the external surface of porous transpiring wall can be regarded as the reactor boundary.

Fig. 8 indicates reactor center temperatures and methanol concentrations under various transpiring wall inner diameters conditions. Apparently, organic feedstock could be rapidly degraded at various transpiring wall inner diameters after entering the reactor. This shows that transpiring wall inner diameter had a slight effect on oxidation reactions of organic feedstock at the same operating parameter conditions [25]. Transpiring wall inner diameter hardly affected reactor center temperatures within $L < 0.025$ m. However, reactor center temperatures reduced with an increase in transpiring wall inner diameter from 0.025 to 0.09 m. This can be explained by the fact that high-temperature reaction zone diffused as transpiring wall inner diameter increased and thus reduced reactor center temperatures. Notably, the influence of inner diameter on reactor center temperature was lower that that of porosity and layer. Reactor center temperature tended to be stable under various transpiring wall inner diameters conditions owing to the stable convection heat transfer between bulk fluid and transpiration water in the lower zone of the reactor ($L > 0.09$ m).

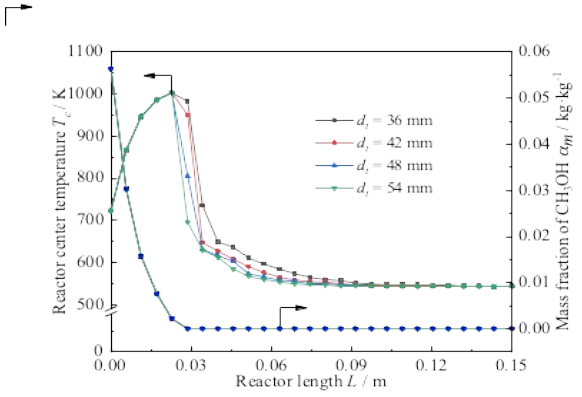

Fig. 8 Reactor center temperatures and methanol concentrations at various transpiring wall inner diameters and

$$p = 23 \text{ MPa}$$

$$Q_m = 0.95 \text{ L} \cdot h^{-1},\ T_{feed} = 753 \text{ K},\ \alpha_m = 20\%, \delta = 0.35,\ T_t = 543 \text{ K}, \chi = 1.25,$$

$$\beta = 0.35, \gamma = 2, \wedge L = 146\, mm.$$

Fig. 9 shows water film temperatures and coverage rates along reactor length under different transpiring wall inner diameters conditions. Evidently, water film temperature reduced with inner diameter increasing in the middle and upper zones of the reactor (L < 0.10 m) but maintained stable in the lower zone (L > 0.10 m). This is in good agreement with the findings in **Fig. 8**. Water film coverage rates raised with an increase in inner diameter in the range of L = 0 – 0.045 m and reached up to about 100% for various inner diameters at L > 0.045 m. This phenomenon can be attributed to the fact that increasing inner diameter expanded the convective heat transfer zone and thus improved heat transfer. Moreover, increasing transpiring wall inner diameter makes water film far away from the central high-temperature zone, thereby reducing water film temperature and enhancing water film continuity. It is noteworthy that increasing transpiring wall inner diameter hardly influenced water film temperature and coverage rate at d_t > 48 mm. Hence, much high inner diameter should be avoided for taking into account the system economy.

Notably, **Fig. 9** displays that water film temperatures reduced while water film coverage rates increased dramatically when the external surface of porous transpiring wall was regarded as the reactor boundary instead of the pressure-bearing wall. This reason may be that transpiration water dissipates when going through the reactor annulus space, which reduces the uniformity and continuity of water film and thus increases water film temperature (see **Fig. 4** and **7**). Hence, the influence of the annulus on reactor performance and water film formation should be paid more attention to in subsequent research.

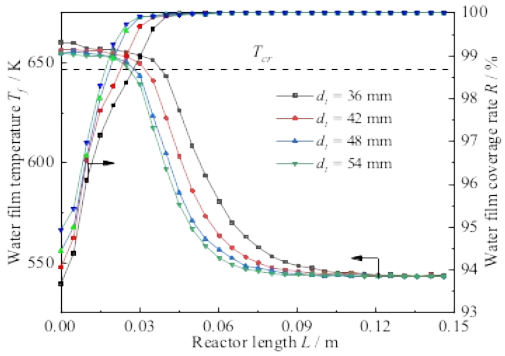

Fig. 9 Water film temperatures and coverage rates at different transpiring wall inner diameters and

p= 23 MPa, Q_m=0.95 L·h^{-1}, T_{feed} = 753 K, α_m=20%, δ=0.35, T_t=543 K, χ=1.25, β=0.35, γ=2, $\wedge L$=

.

三.4 Influence of reactor length

Reactor length (L) represents the axial distance from the reactor top inlet to the bottom outlet, and it affects directly the ranges of upper supercritical oxidation and lower subcritical salt-dissolving zones. **Fig. 10** displays temperature field distributions under various reactor lengths conditions. Apparently, the upper supercritical water oxidation and lower subcritical salt-dissolving zones were formed at different reactor lengths conditions in the TWR. Reactor length had a slight effect on the volume of the upper supercritical oxidation zone, because the upper supercritical oxidation zone is mainly determined by operating parameters of organic feedstock [25]. Notably, increasing reactor length increased the subcritical water film length, thereby improving reactor performance against corrosion and salt deposition. However, this positive effect was limited because reactor temperature tended to be stable in the lower zone for fixed operating parameters [25].

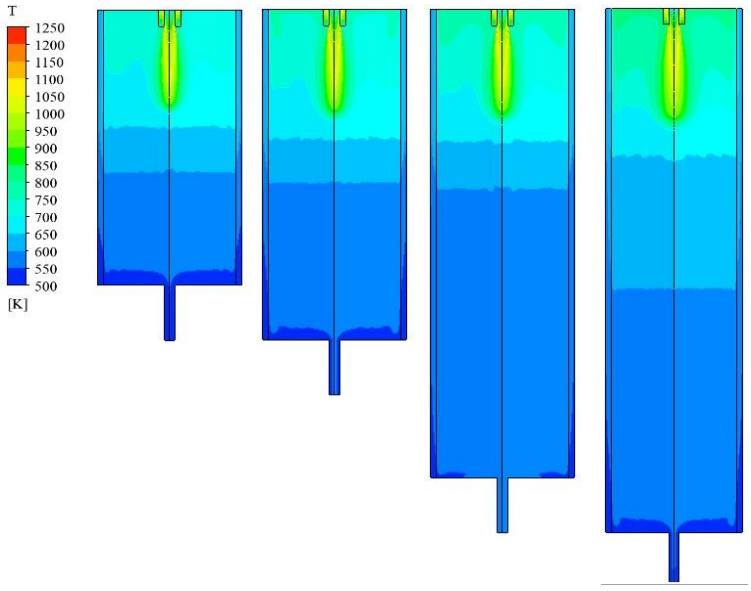

a) b) c) d)

Fig. 10 Temperature field distributions at various reactor lengths and

p= 23 MPa, Q_m=0.95 L·h^{-1}, T_{feed} = 753 K, α_m=20%, δ=0.35, T_t=543 K, χ=1.25, β=0.35, γ=2, $\wedge d_t$=

. (a) L = 50 mm, (b) L = 100 mm (c) L = 170 mm, (d) L = 200 mm.

四 Conclusions

Transpiration water layer, transpiring wall porosity and inner diameter hardly affected methanol degradation. As reactor length increased, reactor center temperature rapidly increased to the maximum value and then gradually reduced and trended to be stable, water film temperature decreased to a stable value, and water film coverage rate increased to near 100% (except for γ=1). Increasing transpiration water layer and transpiring wall porosity reduced reactor center temperature in the middle and lower zones of the reactor, and enlarging transpiring wall inner diameter also decreased it in the middle zone. Increasing transpiration water layer, transpiring wall porosity and inner diameter reduced water film temperature but increased water film coverage rate along reactor length. High-temperature reaction zone approached the reactor top inlet and subcritical salt-dissolving zone expanded with transpiring wall porosity increasing. Prolonging reactor length slightly affected on the volume of the upper supercritical zone but increased that of the subcritical zone.

Author contributions

Peng Feng and Yang Wang contributed equally to this work.

Acknowledgments

This work was supported by the Projects from National Natural Science Foundation of China (22078258), the National Key Research and Development Program of China (2019YFE011926, 2017YFB060360), the Joint Funds of Natural Science Basic Research Plan in Shaanxi Province of China (2019JLM-21), and the Fundamental Research Funds for the Central Universities (xtr042019015, xjh012019005, xzd012020031).

Nomenclature

R = gas constant (J·K^{-1}·mol^{-1})

R_f = water film coverage rate (%)

T = reaction temperature (K)

T_f = water film temperature (K)

T_c = reactor center temperature (K)

T_t = transpiration water temperature (K)

T_{feed} = feed preheating temperature (K)

Q = volume flow rate of fluid (m^3·s^{-1})

Q_m = feed flow rate (L·h^{-1})

Q_t = flow rate of transpiration water (L·h^{-1})

Q_o = flow rate of oxidant (L·h^{-1})

Q_{tot} = total flow rate of fluid (including transpiration water, organic feedstock and oxidant) (L·h^{-1})

δ = transpiration intensity

δ' = thickness of porous transpiring wall (m)

p = static pressure (MPa)

Δp = pressure drop through porous transpiring wall (MPa)

ρ = density ($kg \cdot m^{-3}$)

ρ_{mol} = molar density ($mol \cdot cm^{-3}$)

λ = thermal conductivity ($W \cdot m^{-1} \cdot K^{-1}$)

λ' = thermal conductivity of porous transpiring wall ($W \cdot m^{-1} \cdot K^{-1}$)

λ_f = thermal conductivity of fluid ($W \cdot m^{-1} \cdot K^{-1}$)

λ_s = thermal conductivity of solid ($W \cdot m^{-1} \cdot K^{-1}$)

β = transpiring wall porosity

β' = inertial coefficient

L = reactor length (m)

$L_{¿}$ = supercritical length (m)

$L_{¿}$ = subcritical length (m)

A = pre-exponential factor

A_S = circulation area (m^2)

V_e = pore volume of transpiring wall (m^3)

V_t = total volume of transpiring wall (m^3)

α = viscosity coefficient

α_m = feed concentration (%)

c_p = specific heat capacity at a constant pressure ($J \cdot kg^{-1} \cdot K^{-1}$)

E_a = activation energy ($kJ \cdot mol^{-1}$)

d_t = transpiring wall inner diameter (mm)

χ = oxidation coefficient

D = diffusion coefficient ($m^2 \cdot s^{-1}$)

$A(T)$ $B(T)$ $C(T)$ and $E(T)$ = temperature coefficients

M = molar mass ($g \cdot mol^{-1}$)

μ = dynamic viscosity ($Pa \cdot s^{-1}$)

n = methanol reaction order

m = oxygen reaction order

η = internal resistance coefficient (m^{-1})

ζ = permeability (m^2)

γ = transpiration water layer

References

1. Benjumea JM, Sanchez-Oneto J, Portela JR, Jimenez-Espadafor FJ, Martinez de la Ossa EJ.

Simulation of supercritical water oxidation reactor in transitory state: Application to time-dependent processes. J Supercrit Fluid. 2016;117:219–229.

2. Marrone PA. Supercritical water oxidation—Current status of full-scale commercial activity for waste destruction. *J Supercrit Fluid*. 2013;79:283–288.
3. Xu DH, Huang CB, Wang SZ, Lin GK, Guo Y. Salt deposition problems in supercritical water oxidation. *Chem Eng J*. 2015;279:1010–1022.
4. Xu DH, Wang SZ, Huang CB, Tang XY, Guo Y. Transpiring wall reactor in supercritical water oxidation. *Chem Eng Res Des*. 2014;92(11):2626–2639.
5. Zhang FM, Su CJ, Chen ZY, Chen JL. Experimental study on the mixing characteristics inside an inner preheating transpiring-wall reactor for supercritical water oxidation. *J Supercrit Fluid*. 2020;156.
6. Chen Z, Wang GW, Yin FJ, Chen HZ, Xu YJ. A new system design for supercritical water oxidation. *Che Eng J*. 2015;269:343–351.
7. Xu DH, Wang SZ, Tang XY, Gong YM, Guo Y, Wang YZ, Zhang J. Design of the first pilot scale plant of China for supercritical water oxidation of sewage sludge. *Chem Eng Res Des*. 2012;90(2):288–297.
8. Wellig B, Weber M, Lieball K, Prikopsky K, Von Rohr PR. Hydrothermal methanol diffusion flame as internal heat source in a SCWO reactor. *J Supercrit Fluid*. 2009;49(1):59–70.
9. Zhang FM, Yang J, Ma JN, Su CJ, Ma CY. Optimization of structural parameters of an inner preheating transpiring-wall SCWO reactor. *Chem Eng Res Des*. 2019;141:372–387.
10. Chen Z, Wang GW, Mirza ZA, Yang S, Xu YJ. Study of transpiring fluid dynamics in supercritical water oxidation using a transparent reactor. *J Supercrit Fluid*. 2014;88:117–125.
11. Bermejo MD, Cabeza P, Queiroz JPS, Jiménez C, Cocero MJ. Analysis of the scale up of a transpiring wall reactor with a hydrothermal flame as a heat source for the supercritical water oxidation. *J Supercrit Fluid*. 2011;56(1):21–32.
12. Bermejo MD, Martín A, Queiroz JPS, Bielsa I, Ríos V, Cocero MJ. Computational fluid dynamics simulation of a transpiring wall reactor for supercritical water oxidation. *Che Eng J*. 2010;158(3):431–440.
13. Príkopský K, Wellig B, Von Rohr PR. SCWO of salt containing artificial wastewater using a transpiring-wall reactor: Experimental results. *J Supercrit Fluid*. 2007;40(2):246–257.
14. Xu DH, Guo S, He Z, Huang CB, Jing ZF, Wang SZ. Simulation of a transpiring wall reactor for supercritical water oxidation: Characteristics of water film. *Ind Eng Chem Res*. 2018;57(4):1307–1318.
15. Yakhot V, Orszag SA. Renormalization group analysis of turbulence. I. Basic theory. *J Sci Comput*. 1986;1(1):3–51.
16. Armellini FJ, Tester JW. Solubility of sodium chloride and sulfate in sub- and supercritical water vapor from 450–550°C and 100–250 bar. *Fluid Phase Equilibr*. 1993;84:123–142.
17. Fauvel E, Joussot-Dubien C, Guichardon P, Charbit G, Charbit F, Sarrade S. A double-wall reactor

for hydrothermal oxidation with supercritical water flow across the inner porous tube. *J Supercrit Fluid*. 2004;28(4):47–56.

18. Sandler S. Models for thermodynamic and phase equilibria calculations. *Dekker*. 1995;95:96–101.
19. Liu, HQ, Macedo, EA. Accurate correlations for the self-diffusion coefficients of CO_2, CH_4, C_2H_4, H_20, and D_20 over wide ranges of temperature and pressure. *J Supercrit Fluid*. 1995;8(4):310–317.
20. Mills, KC, Su, YC, Li, ZS, Brooks, RF. Equations for the calculation of the thermo-physical properties of stainless steel. *ISIJ Int*. 2004;44(10):1661–1668.
21. Xu DH, Huang CB, Wang SZ, Guo Y. Characteristics analysis of water film in transpiring wall reactor. *Int J Heat Mass Tran*. 2016;100:559–565.
22. Zhang FM, Ma CY. CFD simulation of a transpiring-wall SCWO reactor: Formation and optimization of the water film. *AIChE J*. 2016;62(1):195–206.
23. Chiu SH, Moore MNJ, Quaife B. Viscous transport in eroding porous media. *J Fluid Mech*. 2020;893.
24. Ren MM, Wang SZ, Roekaerts D. Numerical study of the counterflow diffusion flames of methanol hydrothermal combustion: The real-fluid effects and flamelet analysis. *J Supercrit Fluid*. 2019;152.
25. Kritzer P, Dinjus E. An assessment of supercritical water oxidation (SCWO) : Existing problems, possible solutions and new reactor concepts. *Chem Eng J*. 2001;83(3):207–214.